Role of density-dependent magnon hopping and magnon-magnon repulsion in ferrimagnetic spin-(1/2, S) chains in a magnetic field

W. M. da Silva [1,2] and R. R. Montenegro-Filho [2]
[1]*Secretaria de Educação da Paraíba, 58015-900 João Pessoa-PB, Brazil*
[2]*Laboratório de Física Teórica e Computacional, Departamento de Física, Universidade Federal de Pernambuco, 50760-901 Recife-PE, Brazil*

(Received 9 November 2020; revised 10 February 2021; accepted 10 February 2021; published 22 February 2021)

We compare the ground-state features of alternating ferrimagnetic chains $(1/2,\ S)$ with $S = 1,\ 3/2,\ 2,\ 5/2$ in a magnetic field and the corresponding Holstein-Primakoff bosonic models up to order $\sqrt{s/S}$, with $s = 1/2$, considering the fully polarized magnetization as the boson vacuum. The single-particle Hamiltonian is a Rice-Mele model with uniform hopping and modified boundaries, while the interactions have a correlated (density-dependent) hopping term and magnon-magnon repulsion. The magnon-magnon repulsion increases the many-magnon energy and the density-dependent hopping decreases the kinetic energy. We use density matrix renormalization group calculations to investigate the effects of these two interaction terms in the bosonic model and display the quantitative agreement between the results from the spin model and the full bosonic approximation. In particular, we verify the good accordance in the behavior of the edge states, associated with the ferrimagnetic plateau, from the spin and from the bosonic models. Furthermore, we show that the boundary magnon density strongly depends on the interactions and particle statistics.

DOI: 10.1103/PhysRevB.103.054432

I. INTRODUCTION

The gapped phases of magnetic insulators are responsible for magnetization (m) plateaus in the m vs magnetic field curves [1]. In one dimension, these incompressible phases satisfy the topological Oshikawa-Yamanaka-Affleck [2] criteria and exhibit associated edge states in open spin chains [3]. The gapped phases are separated by gapless phases that have a low-energy physics described by the Tomonoga-Luttinger-liquid theory [4]. Thus, the magnetic field h induces quantum phase transitions in the spin chain, with quantum critical points at the plateau extremes [5,6]. In the vicinity of the quantum critical points, the magnons are in a high-dilute regime and can be treated as a gas of hard-core bosons [7,8] or fermions [9]. In this approximation, the energy is comprised only by a *simple hopping term* and the uniform Zeeman term, which plays the role of chemical potential in the effective model. Following this approach, we can show that the $m(h)$ curve (magnon density) presents a square-root singularity in the gapless side of the transition. The first correction to this law is linear and obtained by taking into account *magnon-magnon interaction* through a phenomenological scattering length [10–14].

Another kind of hopping term is known as *correlated* (or *density-dependent*) *hopping* and is essential in the modeling of a variety of quantum systems [15]. One of these terms, the bond-charge interaction [16], is used to model electrons in strongly correlated materials [17–21] and was particularly investigated in the context of high-T_c superconductivity. Besides, the Hubbard model with this term has an exact solution in a special point of the parameter space [22–25]. On the other hand, the extended boson Hubbard model with a density-dependent hopping is an effective Hamiltonian for bosonic molecules, typically polar species [26–28], in optical lattices [29–36]. Further, general correlated hopping hard-core bosonic Hamiltonians are investigated to understand the physics of frustrated insulating magnetic materials [29–31,37].

The ground state of ferrimagnetic chains satisfies the Lieb-Mattis theorem [38], exhibits ferromagnetic and antiferromagnetic long-range orders [39], and was investigated in the isotropic [40–42] and anisotropic [41,43,44] cases. Ferrimagnetic systems, in particular, the behavior of the edge states associated with the 1/3 magnetization plateau of the AB_2 anisotropic chain, were recently investigated [45]. Furthermore, rich phase diagrams are observed through doping [46–50] or adding geometric frustration [51–58] to the ferrimagnetic models. In particular, ferrimagnetic spin-(1/2, S) chains under an applied magnetic field present magnetization plateaus at $m = S - 1/2$ (ferrimagnetic plateau) and $m = S + 1/2$ (saturation plateau), where m is the magnetization per unit cell [59–64]. On the experimental side, the one-dimensional magnetic phase of a variety of bimetallic compounds was shown to be modeled by spin-(1/2, S) ferrimagnetic chains [65–70]. Recently, the full magnetization curve of the charge-transfer salt (4-Br-o-MePy-V)$FeCl_4$ was experimentally investigated [71] and shown to be a spin-(1/2, 5/2) chain above the three-dimensional ordering temperature.

Since spin-(s, S) ferrimagnetic chains have a long-ranged ordered ground state, linear and interacting spin-wave theory [72] from the classical *ferrimagnetic state* was used to characterize their low-energy magnetic excitations, mainly

through the Holstein-Primakoff formalism [59,60,73–78]. Furthermore, linear spin-wave theory from the *fully polarized state* [64] gives good results for the gapped and gapless phases of spin-$(1/2, S)$ chains in a magnetic field.

Here we show that the Holstein-Primakoff Hamiltonian up to order $\sqrt{s/S}$ gives almost exactly results to the ground-state phase diagram of ferrimagnetic spin-$(1/2, S)$ chains in a magnetic field. We use the density matrix renormalization group (DMRG) [79,80] to obtain the magnetization curves, besides local properties from the Holstein-Primakoff Hamiltonian and the spin Hamiltonian. In addition to the *simple hopping* and the *nearest-neighbor* interacting terms, a *correlated hopping* term is essential to obtain a good accord between the numerical results from the spin and bosonic models. In Sec. II we present the Holstein-Primakoff Hamiltonian and the analytical formulas for the hard-core boson approximation. In Sec. III we compare the DMRG results for the magnetization and local properties from the Holstein-Primakoff Hamiltonian and the spin model. In Sec. IV we present a summary of the main results of the paper.

II. HOLSTEIN-PRIMAKOFF BOSONIC HAMILTONIAN FROM THE FULLY POLARIZED VACUUM

The alternating mixed-spin $(s = 1/2,\ S)$ chain with L unit cells has the Hamiltonian

$$\mathcal{H}^{\text{SPIN}} = J\sum_{j=1}^{L}(\mathbf{s}_j\cdot\mathbf{S}_j + \mathbf{s}_j\cdot\mathbf{S}_{j-1}) - BS^z_{\text{tot}}, \tag{1}$$

where

$$S^z_{\text{tot}} = \sum_j \left(s^z_j + S^z_j\right) \tag{2}$$

is the z component of the total spin, and we consider the magnetic field B in the z direction, with $g\mu_B \equiv 1$, where μ_B is the Bohr magneton and g is the g factor. The spin-1/2 are attached to a sites, while spin-S to b sites along the chain, and we study chains for which $S = 1,\ 3/2,\ 2,\ 5/2$, as schematically shown in Fig. 1(a). The ground-state total spin for $B = 0$ is $S - s$ and has a copy in each sector in the range $-(S-s) \leqslant S^z_{\text{tot}} \leqslant (S-s)$, as expected from the Lieb-Mattis theorem [38], with a ferrimagnetic (FRI) long-range ordered state. If a little magnetic field is applied, the ground state with $S^z_{\text{tot}} = (S-s)$ is chosen. Further, the ground state has a finite gap to spin excitations carrying a spin $\Delta S^z = +1$, which induces a magnetization plateau at $m_{\text{FRI}} = (S-s)$. Also, a second magnetization plateau is the fully polarized plateau at $m_{\text{FP}} = S + s$.

The *fully polarized state* is an exact ground state of the spin Hamiltonian, and we build the spin-wave theory considering it as the magnon vacuum. Making the Holstein-Primakoff mapping on a sites

$$\begin{aligned} s^z_j &= s - n^a_j, \\ s^-_j &= \sqrt{2s}a^\dagger_j\left(1 - \frac{n^a_j}{2s}\right)^{1/2} \approx \sqrt{2s}a^\dagger_j\left(1 - \frac{n^a_j}{4s}\right), \end{aligned} \tag{3}$$

and on b sites:

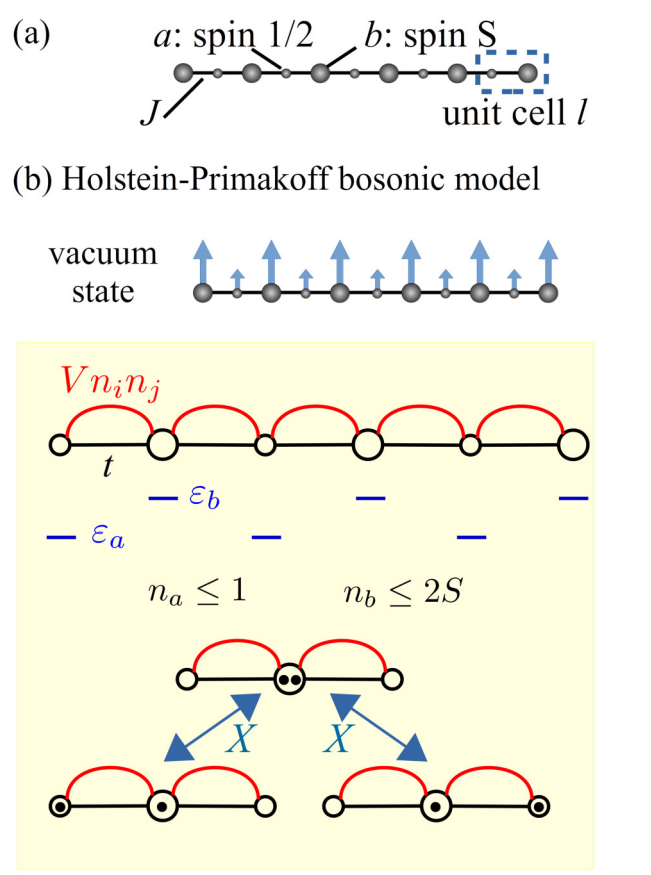

FIG. 1. (a) Schematic representation of the alternating spin model, with spin-1/2 at a sites, and spin-S at b sites, with $S = 1,\ 3/2,\ 2$, and $5/2$. The z direction is the direction of an applied magnetic field B and the superexchange coupling is J. (b) Holstein-Primakoff bosonic Hamiltonian up to $\mathcal{O}(S^{-1/2})$, with a hopping term $t = J\sqrt{sS}$, local potentials $\varepsilon_a = -2SJ$ and $\varepsilon_b = -2sJ$, nearest-neighbor interaction $V = J$, and density dependent correlated hopping process $X = J\sqrt{s/S}$. The a sites have a hard-core constraint, $n_a \leqslant 1$, while the constraint $n_b \leqslant 2S$ is imposed on b sites, with n_a (n_b) as the number of bosons in one a (b) site. The magnetic field B acts as a chemical potential μ in the bosonic model: $\mu = -B$. (c) The bosonic approximations investigated: t, t-V, and t-X-V. In the t and t-V approximations, there is a hard-core constraint on all sites, while in the t-X-V model, the b sites can accommodate up to two magnons.

$$\begin{aligned} S^z_j &= S - n^b_j; \\ S^-_j &= \sqrt{2S}b^\dagger_j\left(1 - \frac{n^b_j}{2S}\right)^{1/2} \approx \sqrt{2S}b^\dagger_j\left(1 - \frac{n^b_j}{4S}\right), \end{aligned} \tag{4}$$

where $n^a_j = a^\dagger_j a_j$ and $n^b_j = b^\dagger_j b_j$, we arrive in the following spin-wave Hamiltonian

$$\mathcal{H}^{\mathrm{SW}} = J\sum_j \Big\{ (S-n_j^b)(s-n_j^a) + \sqrt{sS}\Big[\Big(1-\frac{n_j^b}{4S}\Big) b_j a_j^\dagger \Big(1-\frac{n_j^a}{4s}\Big) + b_j^\dagger \Big(1-\frac{n_j^b}{4S}\Big)\Big(1-\frac{n_j^a}{4s}\Big) a_j\Big] + \sqrt{sS}\Big[\Big(1-\frac{n_j^a}{4s}\Big) a_j b_{j+1}^\dagger \Big(1-\frac{n_{j+1}^b}{4S}\Big) + a_j^\dagger \Big(1-\frac{n_j^a}{4s}\Big)\Big(1-\frac{n_{j+1}^b}{4S}\Big) b_{j+1}\Big] + (s-n_j^a)(S-n_{j+1}^b)\Big\} - B\sum_j \big(S+s-n_j^a-n_j^b\big) + \mathcal{O}(S^{-1}). \tag{5}$$

Dropping the classical energy of the ferromagnetic state $E_{\mathrm{class}} = 2JLsS - B(S+s)L$, the relevant magnon Hamiltonian is:

$$H^{\mathrm{SW}} = H_t + H_X + H_V + \mathcal{O}(S^{-1}), \tag{6}$$

with $H^{\mathrm{SW}} = \mathcal{H}^{\mathrm{SW}} - E_{\mathrm{class}}$.

As sketched in Fig. 1(b), the H_t term comprises a hopping process and distinct local potentials on a and b sites:

$$H_t = t\sum_j (b_j^\dagger a_{j+1} + b_{j+1}^\dagger a_{j+1} + \mathrm{H.c.}) + \sum_j [(\varepsilon_a-\mu)n_j^a + (\varepsilon_b-\mu)n_j^b] \tag{7}$$

with

$$\begin{aligned} t &= J\sqrt{sS}, \quad \text{hopping parameter;}\\ \varepsilon_a &= -2SJ, \quad \text{local potential on } a \text{ sites;}\\ \varepsilon_b &= -2sJ, \quad \text{local potential on } b \text{ sites;}\\ \mu &= -B. \end{aligned} \tag{8}$$

In an open chain, if a or b is a boundary site, the local potential is half of the above value:

$$\begin{aligned} \varepsilon_a^{(\mathrm{boundary})} &= -SJ\\ \varepsilon_b^{(\mathrm{boundary})} &= -sJ. \end{aligned} \tag{9}$$

Considering the local potentials, we see that the magnon has a higher probability to be found on a sites, and this probability increases with S. However, since the hopping parameter t increases with $\sqrt{S}$, quantum fluctuations are relevant for moderate values of S, and the magnons can overcome the potential barrier between a and b sites.

We observe that the bulk Hamiltonian H_t is a particular case of the Rice-Mele model [81]:

$$H^{\text{Rice-Mele}} = \sum_j (t_2 b_j^\dagger a_{j+1} + t_1 b_{j+1}^\dagger a_{j+1} + \mathrm{H.c.}) + \sum_j \big(\varepsilon_a n_j^a + \varepsilon_b n_j^b\big), \tag{10}$$

putting $\mu = 0$ and considering the general case of alternating hopping: t_1 (t_2) for intracell (intercell) hopping. The Rice-Mele Hamiltonian was originally proposed to model the physics of electrons in polymers but is a paradigmatic model to the understanding of topological insulators and can be realized by atoms in optical lattices [82]. The model presents the bulk-boundary correspondence [83], and an interacting version was recently investigated [83] to probe the connection between topology and particle-particle interactions [83]. The Rice-Mele model recovers the bulk Hamiltonian H_t for $t_1 = t_2$. However, for an open chain, the mapping of the spin model requires local potentials on the boundary sites, Eq. (9).

The second term in the bosonic Hamiltonian (6) is a density-dependent or correlated hopping term given by

$$H_X = -X\sum_j \big[(a_j^\dagger + a_{j+1}^\dagger) n_j^b b_j + \mathrm{H.c.}\big], \tag{11}$$

with

$$X = \frac{J}{4}\sqrt{\frac{s}{S}}. \tag{12}$$

Since $s = 1/2$ and $n_j^a \leqslant 1$, a hard-core constraint must be imposed on a sites for all models considered. Hence, we discard a term similar to the X term but with a and b variables exchanged, with $X' = \frac{J}{4}\sqrt{S/s}$ as the correlated hopping amplitude. As sketched in Fig. 1(b), the energy of the system is lowered by the hopping of a magnon to a site that is already occupied. In other words, the magnon probability to overcome the potential barrier between a and b sites increases if there is one magnon on the b site. This term becomes relevant for higher magnon densities, since it is an interaction term, and $X \to 0$ as S increases.

The last term in the Hamiltonian (6), see Fig. 1(b), is a repulsive term between magnons in nearest neighbor sites:

$$H_V = V\sum_j n_{j+1}^a \big(n_j^b + n_{j+1}^b\big), \tag{13}$$

with $V = J$, and increases the energy for higher magnon densities. For one magnon per unit cell, this term favors the magnon localization on alternating a sites, since the local potentials (ε) favor the occupation of a sites. Thus, ε (any density) and V (higher densities) favor magnon localization on a sites, while quantum fluctuations (tunneling between a and b sites) are favored by t (any density) and X (higher densities).

In this work, we compare data from three approximations of Hamiltonian (6), as summarized in Fig. 1(c), and from the spin Hamiltonian (1). The first, which we identify as the t approximation, is an analytical solution to the free hard-core model. In this approximation, all sites have a hard-core constraint and can be occupied by only one magnon: $n_j^a \leqslant 1$ and $n_j^b \leqslant 1$, for any j. This constraint implies that there is not an energy contribution from the X term, and we drop the nearest-neighbor interaction V. In the second approximation, t-V, we keep the hard-core constraint but add the V contribution to H_t. The last approximation, t-X-V, has the three terms H_t, H_X,

and H_V. We consider a hard-core constraint on a sites and a constraint $n_j^b \leqslant 2$ on b sites. As we present below, the relaxation of the hard-core constraint on b sites and the consequent activation of the correlated hopping term implies an excellent agreement between the results of this approximation and the spin model.

A. Free hard-core magnons (t approximation): H_t and $L \to \infty$

The first approximation to the magnetization curve, a many-magnon state, is to consider the magnons as free hard-core bosons or free fermions. This mapping is exact in the high-dilute regime of magnons, near the saturation field. Here, we extend this approach for the full range of the magnetization, $(S-s) \leqslant m \leqslant (S+s)$, and compare their results to more precise calculations considering the interaction terms.

The single-magnon energies are given by the term H_t, Eq. (7), in Hamiltonian (6). Using the following Fourier transforms:

$$a_j = \frac{1}{\sqrt{L}} \sum_k e^{-ik/4} e^{ikj} a_k;$$
$$b_j = \frac{1}{\sqrt{L}} \sum_k e^{+ik/4} e^{ikj} b_k, \tag{14}$$

where a phase $e^{\pm ik/4}$ is included to ease the calculation, H_t becomes:

$$H_t = \sum_k \begin{pmatrix} a_k^\dagger & b_k^\dagger \end{pmatrix} \begin{pmatrix} \varepsilon_a & \gamma_k \\ \gamma_k & \varepsilon_b \end{pmatrix} \begin{pmatrix} a_k \\ b_k \end{pmatrix}, \tag{15}$$

where

$$\gamma_k = 2t \cos(k/2). \tag{16}$$

After diagonalization, the Hamiltonian is written as

$$H_t = \sum_k \omega_k^{(-)} n_k^{(-)} + \omega_k^{(+)} n_k^{(+)}, \tag{17}$$

where the dispersion relations are

$$\omega_k^{(\pm)} = \frac{\varepsilon_a + \varepsilon_b}{2} \pm \omega_k = -J(s+S) \pm \omega_k, \tag{18}$$

with

$$\omega_k = \sqrt{\left(\frac{\varepsilon_b - \varepsilon_a}{2}\right)^2 + \gamma_k^2}$$
$$= J\sqrt{(S-s)^2 + 4sS\cos^2(k/2)}, \tag{19}$$

and $n_k^{(\pm)} = \alpha_k^{(\pm)\dagger} \alpha_k^{(\pm)}$, where

$$\begin{pmatrix} \alpha_k^{(-)} \\ \alpha_k^{(+)} \end{pmatrix} = \begin{pmatrix} \cos\theta_k & -\sin\theta_k \\ \sin\theta_k & \cos\theta_k \end{pmatrix} \begin{pmatrix} a_k \\ b_k \end{pmatrix}, \tag{20}$$

with

$$\cos^2\theta_k = \frac{1}{2} + \frac{S-s}{2\omega_k};$$
$$\sin^2\theta_k = \frac{1}{2} - \frac{S-s}{2\omega_k}. \tag{21}$$

A magnetic field (or chemical potential) adds a $+B$ energy term to the two bands.

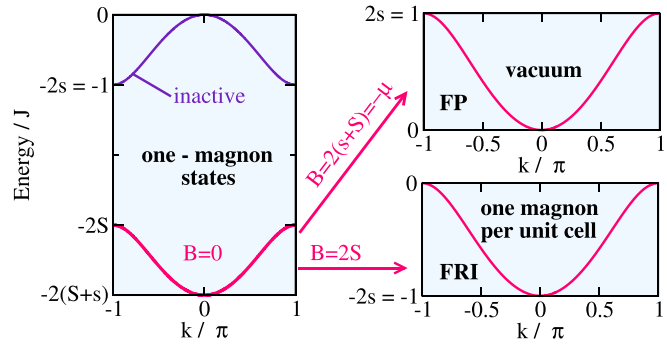

FIG. 2. One-magnon states from the fully polarized (FP) vacuum and $B = 0$ as a function of lattice wave vector k. In the t approximation, the high energy band is inactive. For $B = 2(s+S) = -\mu$, the exact ground state is the FP vacuum, while there is one magnon per unit cell in the system for $B = 2S$, and the ground state is ferrimagnetic (FRI).

The magnon bands are shown in Fig. 2 for (i) $B = 0$; (ii) $B = 2(s+S)$, the saturation field, for which $m = m_{\rm FP} = (S+s)$; (iii) $B = 2S$, the critical field of the ferrimagnetic plateau, for which $m = m_{\rm FRI} = (S-s)$, or 1 magnon per unit cell: $m_{\rm FP} - m_{\rm FRI} = (S+1/2) - (S-1/2) = 1$. As expected from the Lieb-Mattis theorem, the magnetization in the null field is $S-s$. In the free hard-core boson or free fermion approximation, we fill the single-particle states following a Fermi distribution up to the effective Fermi wave vector k_F. As shown in Fig. 2, if we follow this procedure the two bands should be filled for $B = 0$ (two magnons per unit cell) and the magnetization curves of the spin model would not be reproduced. We have shown in Ref. [64] that this problem can be overcome, even for finite T, by introducing an effective chemical potential μ to the upper band, in a way similar to Takahashi's solution to the ferromagnetic linear chain [84]. In particular, $\mu \to -J = -2sJ$ as $T \to 0$, such that the overall effect of μ at $T = 0$ is the suppression of the upper band. Hence, in the free hard-core approximation, we must consider only the lower band in the calculations, as schematically indicated in Fig. 2. Thus, for example, the energy per unit cell in the free hard-core approximation is written as

$$\frac{E}{L} = \frac{1}{L} \sum_{k=-k_F}^{k_F} \omega_k^{(-)} \tag{22}$$

for a magnon density per unit cell n, where

$$k_F = \pi n, \tag{23}$$

and $n = m_{\rm FP} - m$.

1. Average local magnetizations

If the chain has a magnon density per unit cell n and considering the hard-core approximation, the average magnetizations of a and b sites are given by

$$\langle s^z \rangle = s - \frac{1}{L} \sum_{k=-k_F}^{k_F} \langle n_k^a \rangle \quad (a \text{ sites});$$
$$\langle S^z \rangle = S - \frac{1}{L} \sum_{k=-k_F}^{k_F} \langle n_k^b \rangle \quad (b \text{ sites}). \tag{24}$$

Using Eqs. (20) and discarding terms involving the upper band, we obtain

$$\langle n_k^a \rangle = n_k^{(-)} \cos^2\theta_k;$$
$$\langle n_k^b \rangle = n_k^{(-)} \sin^2\theta_k. \quad (25)$$

We thus have

$$\langle s^z \rangle = s - \frac{1}{2} - \frac{S-s}{2} \sum_{k=-k_F}^{k_F} \frac{1}{\omega_k};$$
$$\langle S^z \rangle = S - \frac{1}{2} + \frac{S-s}{2} \sum_{k=-k_F}^{k_F} \frac{1}{\omega_k}, \quad (26)$$

after the substitution of Eqs. (21) in Eqs. (25) and the results in Eqs. (24).

III. DMRG RESULTS FOR THE SPIN MODEL AND THE BOSONIC HAMILTONIANS

A. Methodology

We use the density matrix renormalization group to obtain the magnetization curves and local properties of the spin, t-V, and t-X-V models and also compare this data with the analytical results from the free hard-core model (t model) in the thermodynamic limit: $L \to \infty$. These approximations are summarized in Fig. 1(c). All DMRG results (boson and spin models) are obtained through the Algorithms and Libraries for Physics Simulations (ALPS) project [85] for chains with $L = 128$ unit cells, with one a site at one extreme and a b site at the other. If the system has an a site at the left extreme and a b in the right (a-b boundaries), the renormalization process for the magnetization step inside the ferrimagnetic plateau becomes trapped in a metastable state for $S = 3/2,\ 2,$ and $5/2$. In these cases, the global energy minimum is reached by the algorithm if the chains have a b site at the left extreme and an a site at the right extreme (b-a boundaries). In the other magnetizations, this is irrelevant, i.e., the same state is calculated for the a-b or the b-a boundaries. We retain a maximum of 243 states per block and the maximum discarded weight less than 10^{-9}.

For the spin model, the magnetization curves are calculated from the lowest energy state for a fixed S^z and $B = 0$: $E(S^z)$, since for $B \neq 0$ we need only to add the Zeeman term, such that $E_B(S^z) = E(S^z) - BS^z$. In a gapless (nonplateau) phase, the magnetization curves are made of finite steps in a finite-size system. Defining the extreme points of these finite steps as B_- and B_+, we have

$$B_\pm = \pm[E(S^z \pm 1) - E(S^z)] \quad (27)$$

for the step at S^z. In a gapless phase, $B_- \to B_+$ as $L \to \infty$, while in a thermodynamic-limit plateau state $B_- \neq B_+$ for $L \to \infty$. In the last case, $B_\pm$ are quantum critical fields separating the plateau insulating state from a gapless critical Luttinger liquid phase. For the bosonic models, the magnon density per unit cell n as a function of chemical potential μ is obtained with a similar procedure. We calculate the lowest energy state for a fixed number of bosons N, with $N = nL$ and $\mu = 0$. The value of the chemical potential at the extremes

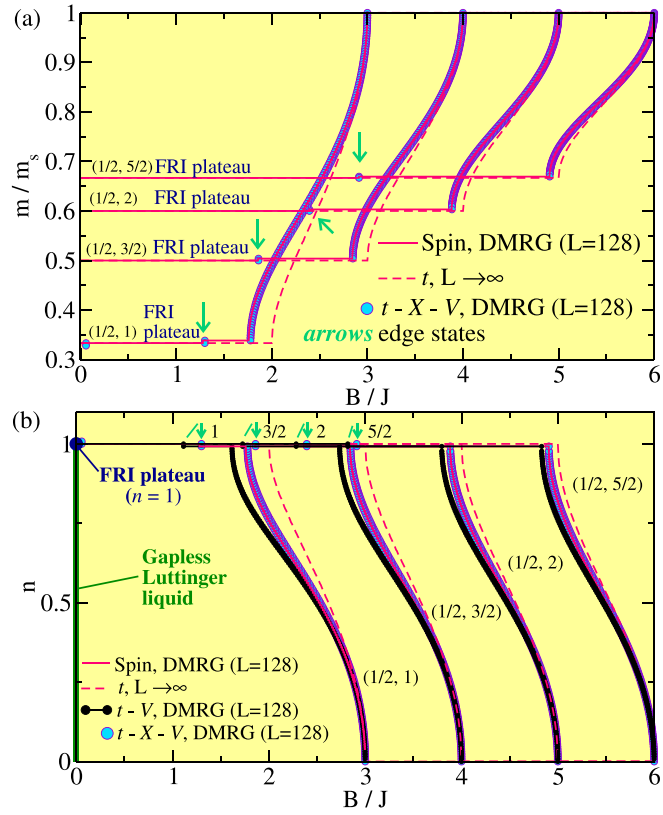

FIG. 3. (a) Magnetization per unit cell (m) of $(1/2,\ S)$ chains, with $S = 1,\ 3/2,\ 2,$ and $5/2$, normalized by its saturation value (m_s) and (b) magnon densities per unit cell n as functions of B in units of J. DMRG data for (full lines) the spin model and for (•) the t-X-V approximation. We present in both figures the results for the t model (dashed lines) and $L \to \infty$. In (b), we also show the magnon density as a function of B units of J for (•) the t-V approximation, calculated with DMRG for a system with $L = 128$. In the thermodynamic limit, the ferrimagnetic plateau is observed for $n = 1$, while the gapless Luttinger liquid phase for $0 < n < 1$. On both figures, we indicate (arrows) the magnetic field at which the edge states are occupied by one magnon.

(μ_- and μ_+) of the step at N are given by

$$\mu_\pm = \pm[E(N \pm 1) - E(N)]. \quad (28)$$

A gapless phase has $\mu_+ \to \mu_-$ as $L \to \infty$, while in a plateau insulating phase $\mu_+ \neq \mu_-$ in the thermodynamic limit. The transformation from the boson to the spin language is performed through the following equations:

$$n = m - m_{\rm FP}, \text{ and}$$
$$B = -\mu. \quad (29)$$

B. Magnetization curves and local magnetizations

The magnetization curves from the spin model and the boson Hamiltonians are shown in Fig. 3(a). The models present two magnetization plateaus, one at the ferrimagnetic magnetization $m_{\rm FRI} = S - 1/2$ and the fully polarized state $m_{\rm FP} = S + 1/2$. The saturation field B_{FP}, end point of the FP plateau, is obtained through the closing of the single-particle magnon gap with B, as sketched in Fig. 2, at $B = B_{\rm FP} = 2(S + s)$.

The saturation field $B_{\rm FP}$ from any bosonic approximation is rigorously equal to its exact value since the fully polarized state, an exact eigenstate of the spin model, is the vacuum for the bosonic models.

The Oshikawa-Yamanaka-Affleck topological criteria [2] states that a plateau can appear in the magnetization curve of spin systems if

$$S_u - m = \text{integer}, \tag{30}$$

where S_u is the maximum spin of a unit cell, unless the ground state spontaneously breaks translation symmetry. This corresponds to a number of magnons per unit cell $n = 0, 1, 2, \ldots, S_u(S_u - 1/2)$ for integer (half integer) S_u, from the fully polarized state. Since $S_u = S + 1/2$ (saturated magnetization) for spin-$(1/2, S)$ chains, plateaus could appear at $m = S + 1/2, (S - 1/2), \ldots, 0(1/2)$, for half integer (integer) S. In the spin-$(1/2, S)$ chains, the data shows that there are two magnetization plateaus, one at the fully polarized ($n = 0$) magnetization and the other at one magnon per unit cell ($n = 1$), the ferrimagnetic plateau. The other possible magnetization plateaus are inhibited by the magnon-magnon interaction term V [Eq. (13)]. The magnetization curves of ferrimagnetic spin chains with $1/2 < s < S$ can exhibit other plateaus between the ferrimagnetic and the fully polarized ones. This is observed, for example, in spin-(1, 2) and spin-(1, 3/2) chains [86]. For these chains, the ferrimagnetic plateau state has two magnons per unit cell, $n = 2$, and the magnetization curves also exhibit a plateau at $n = 1$. We also observe the occupancy of the edge states of the ferrimagnetic plateau by one magnon at the indicated magnetic fields. These edge states appear in finite-size open systems associated with topological aspects [3,45] of the ferrimagnetic state.

The noninteracting Rice-Mele model (10) does not present edge states for uniform hopping. However, recently [83], it was shown that an interacting *fermionic system*, with a local Coulomb interaction, presents effective edge states, and that a fraction of the boundary charge is, in fact, related to the bulk properties. Our noninteracting Hamiltonian (7) has the modified local potentials in the boundaries (9), required from the spin mapping, and thus localized edge states. Furthermore, our interacting model is a *bosonic system* having the correlated hopping and nearest-neighbor Coulomb repulsion. In Sec. IV, we study the boundary magnon density and compare it from relevant interacting and noninteracting bosonic models. The gapless phase between the magnetization plateaus is a Luttinger liquid phase with power-law decay of the transverse spin correlation functions [4] and has a dynamical exponent $z = 1$.

We notice in Fig. 3(a) that as B decreases from $B_{\rm FP}$, the magnetization from the free hard-core model, t approximation, departs from that of the spin model at roughly half filling of the lower magnon band $\omega^{(-)}$, Eq. (18). At this filling, the interaction effects start to become relevant. The critical field of the ferrimagnetic plateau from the free hard-core model: $2S$, see Fig. 2, becomes more near its value for the spin model as S increases, as also confirmed in Table I. This effect can be attributed to the local energy of the a sites that becomes deeper in comparison with the local energy of the b sites, as can be seen in the energy term (7) and the sketch in Fig. 1. Thus, the magnons become more localized on a sites as S increases,

TABLE I. Critical field of the ferrimagnetic plateau in units of J for the spin-$(1/2, S)$ chains in the free hard-core boson approximation t approximation and the spin model.

S	t approx.: $2S$	spin model: β	$\frac{2S-\beta}{\beta}$
1	2	1.76	0.13
3/2	3	2.85	0.05
2	4	3.88	0.03
5/2	5	4.91	0.02

and the X and V energy terms, Eqs. (11) and (13), respectively, become lesser relevant. The X term due to the low occupancy probability of one b site by two magnons and also because $X \to 0$ as $S \to \infty$, see Eq. (12). The V term, on the other hand, because the probability of finding two magnons in nearest neighbor sites is also very low. Further, the t-X-V approximation, which has all energy terms in Hamiltonian (6) active, is in excellent agreement with the results for the spin model. Even the location of the edge states is well reproduced by the t-X-V approximation.

In Fig. 3(b) we show the average magnon density per unit cell $\langle n \rangle$. Besides the models presented in (a), we add the t-V approximation. The presence of the magnon repulsion makes the accordance with the spin model good for $\langle n \rangle > 1/2$, while in the t approximation this agreement is good up to a value of $\langle n \rangle$ less than $1/2$. As $\langle n \rangle \to 1$, reaching the ferrimagnetic plateau, the repulsion V increases much the energy of the system and thus implies a lower value of the critical magnetic field $B_{\rm FRI}$, compared to the spin model. The location of the edge states in the finite-size system is also different between the spin and the t-V approximation. Further, the X term, the density-dependent hopping term, lowers the energy, and the full $\langle n \rangle$ curve of the spin model is well reproduced by the t-X-V approximation. We notice, however, that only for the finite size spin-$(1/2, 1)$ chain studied, the lower critical field of the ferrimagnetic plateau is $B \approx 0.06J$. In Sec. IV, we present the magnon curve for $N > 128$.

The average spin and magnon density at a and b sites are shown in Fig. 4. Notice that the average spin at b sites, Fig. 4(b), is normalized by S. Also shown are the probability of occupancy of a and b sites. We use the expressions (26) to obtain the average spins from the t approximation, while we calculate the average magnon density from the spin model with

$$\langle n_a \rangle = \frac{1}{2} - \frac{1}{L}\sum_{l=1}^{L} \langle s_l^z \rangle,$$

$$\langle n_b \rangle = S - \frac{1}{L}\sum_{l=1}^{L} \langle S_l^z \rangle, \tag{31}$$

for a finite spin chain of size L and open boundaries. The value of the average spin at a sites from any of the considered bosonic approximations is in good agreement with its value from the spin model. A relevant departure between the approximations and the spin model occurs in the average spin on b sites as the ferrimagnetic magnetization plateau is approached. However, even the t approximation provides

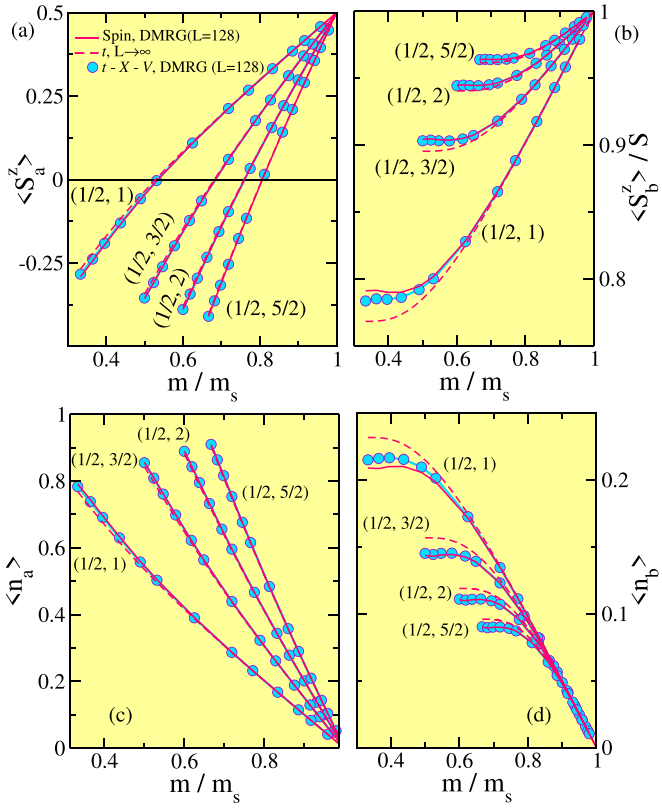

FIG. 4. Average spin at (a) a, $\langle S^z_a\rangle$, and (b) b, $\langle S^z_b\rangle$, sites, in this case normalized by S, for $(1/2, S)$ chains with $S = 1, 3/2, 2$, and $5/2$, as a function of the normalized magnetization m/m_s, where m_s is the saturation magnetization of each chain. The hard-core boson t approximation in the thermodynamic limit (dashed lines), DMRG results for the spin model (full lines) and the t-X-V approximation (•), both for systems with $L = 128$. Average magnon densities at (c) a, $\langle n_a\rangle$, and (d) b, $\langle n_b\rangle$, sites as a function of m/m_s and the same legend of (a) and (b).

good values for the average spins, as shown in Table II for the ferrimagnetic magnetization. Also, the results become indistinguishable, even on b sites, as S increases or as the fully polarized plateau is approached. Furthermore, as in the magnetization results, the t-X-V model is an excellent approximation to the spin Hamiltonian. The data in Figs. 4(c) and 4(d) confirm that due to the higher value of the local potential on a sites, the probability of occupancy of a sites is higher than that on b sites, as discussed in the context of the magnetization curves in Fig. 3. In particular, quantum fluctuations are reduced as S increases, since $\langle n_b\rangle \to 0$ in this limit, as the data in Fig. 4(d) suggests.

TABLE II. Average spins at a ($\langle s^z\rangle$) and b ($\langle S^z\rangle$) sites for the spin-$(1/2, S)$ chains in the free hard-core boson approximation t and the spin model: ($\langle s^z\rangle$, $\langle S^z\rangle$), at $m = S - s$, the ferrimagnetic magnetization.

S	t approx.	Spin model
1	(−0.27, 0.77)	(−0.29, 0.79)
3/2	(−0.34, 1.34)	(−0.36, 1.36)
2	(−0.38, 1.88)	(−0.39, 1.89)
5/2	(−0.40, 2.40)	(−0.41, 2.41)

In Figs. 5(a) and 5(b) we present the local magnon densities in finite chains with open boundaries for the spin and the t-X-V models. The magnon densities from the spin model are calculated through

$$\langle n^a_l\rangle = \tfrac{1}{2} - \langle s^z_l\rangle;$$
$$\langle n^b_l\rangle = S - \langle S^z_l\rangle, \tag{32}$$

and $\langle n^{\rm cell}_l\rangle = \langle n^a_l\rangle + \langle n^b_l\rangle$. We show the data for the spin-$(1/2, 1)$ and spin-$(1/2, 5/2)$ chains, for two low magnon densities ($n = 8/128$, $n = 16/128$), near the fully polarized magnetization plateau, and two high magnon densities, more near the ferrimagnetic magnetization plateau ($n = 72/128$, $n = 116/128$), in a chain with $L = 128$ unit cells. For the lower magnon densities (hard-core limit) the results for t-X-V approximation departs from the spin model data near the boundaries for the spin-$(1/2, 1)$. However, the accordance between the two models is excellent in the case of the spin-$(1/2, 5/2)$, even near the boundaries, for the two lower magnon densities shown. For the two higher magnon densities, there is an excellent agreement between the spin model and the t-X-V approximation for the two chains.

In Fig. 5(c), we show the magnon distribution in the edge localized state occupied by one magnon for the four chains studied. To calculate it, we notice that the edge state appears between the two magnetization steps: $S^z = L(S - s)$ and $S^z = L(S - s) + 1$, which will join in the thermodynamic limit, and make the $S - s$ ferrimagnetic plateau, see Fig. 3(a) and 3(b). Thus, to visualize the spatial extent of the edge state, we consider the magnon distribution change, $\delta\langle n\rangle_{\rm FRI+1\to FRI}$, between a total number of magnons $N = L - 1$ [$S^z = L(S - s) + 1$] and $N = L$ [$S^z = L(S - s)$]:

$$\delta\langle n\rangle_{{\rm FRI+1}\to{\rm FRI},l} = \langle n\rangle_{N=L,l} - \langle n\rangle_{N=L-1,l}. \tag{33}$$

We notice in the data shown in Fig. 5(c) that a tiny discrepancy is observed between the results for the t-X-V-approximation and the spin model in the case of the $(1/2, 1)$ chain, while for the other chains the agreement is excellent. The hole added to the many-magnon state at $N = L$ becomes well localized in the boundary cell, mainly on the boundary a site, thus implying the presence of this empty orbital in the $N = L - 1$ [$S^z = L(S - s)$] state. The localization in the boundary increases with S as expected from the increasing of the bulk gap. In fact, the fluctuations of the magnon density in the boundary become negligible as $S \to \infty$, and the boundary hosts one magnon in this limit. We can attribute this behavior to the increasing potential barrier between bulk and edge, Eqs. (8) and (9), respectively, as $S \to \infty$.

As an example of the data used to make the results shown in Fig. 5(d), we exhibit in Fig. 5(d) the average magnon density along the chain, $\langle n\rangle$, for a and b sites, in the t-X-V approximation of the $(1/2, 1)$ chain. We notice that the a site at the left boundary is almost empty for $N = L - 1$, while its $\approx$0.6 for $N = L$, implying the value shown in (c). We also notice a sizable change in the occupation of the b site at the left boundary for the two fillings, while $\langle n\rangle$ does not change at the right boundary. A sketch of the two ground states is shown in Fig. 5(e). For $N = L - 1$, we have an insulating state

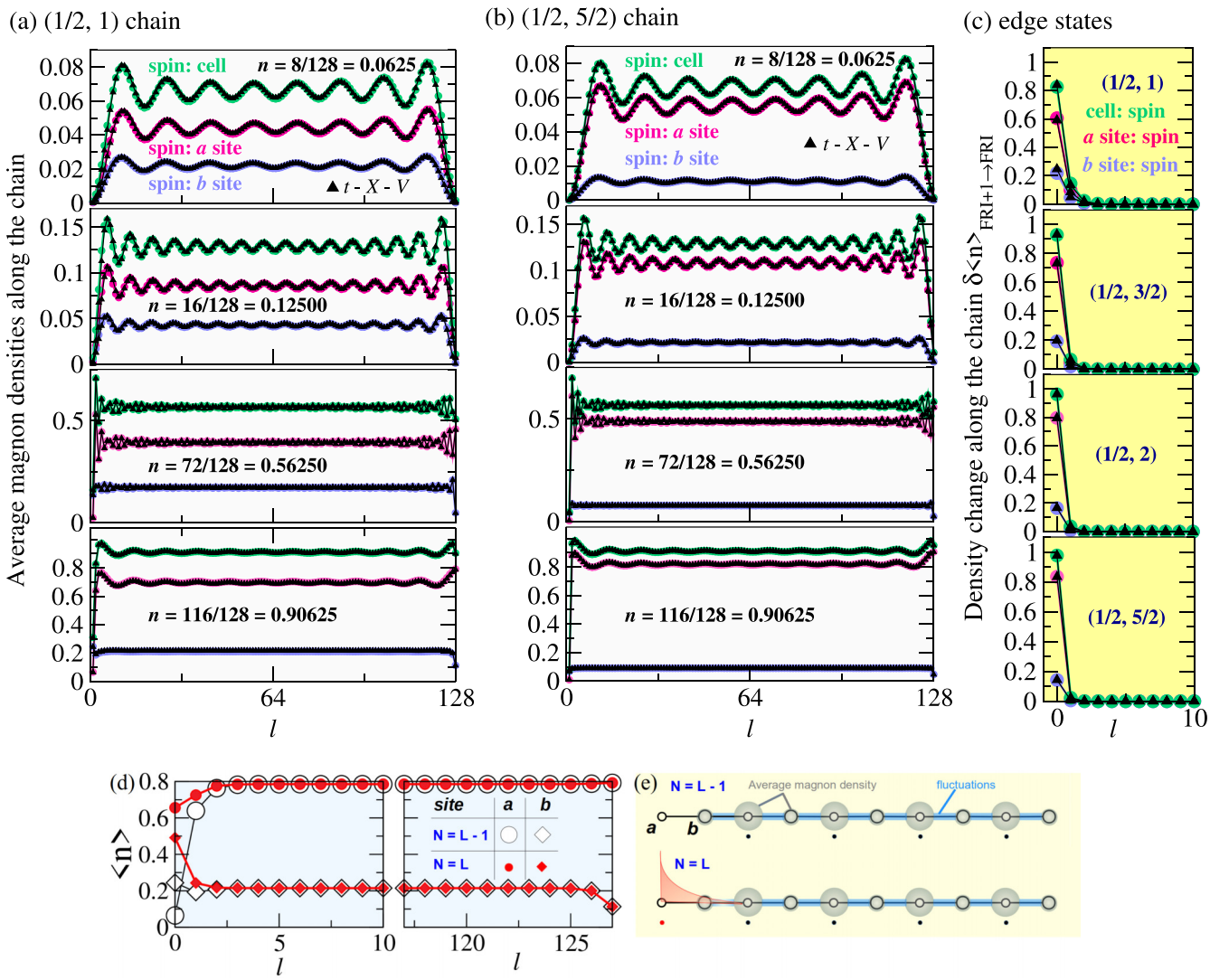

FIG. 5. Average magnon densities along (a) the $(1/2, S = 1)$ chain and (b) the $(1/2, S = 5/2)$ with $L = 128$ unit cells. Magnon densities at (pink •) a sites, $\langle n_{a,l}\rangle$, at (purple •) b sites, $\langle n_{b,l}\rangle$, and (green •) total magnon density, $\langle n_{\text{cell},l}\rangle$, for unit cell l from the spin model and (▲) the t-X-V approximation, both calculated with DMRG for systems with $L = 128$. The following total average magnon densities are shown: $n = 8/128$, $16/128$, $72/128$, and $116/128$, from top to bottom, corresponding, respectively, to the magnetizations (a) $m = 184/128$, $176/128$, $120/128$, and $76/128$ and (b) $m = 376/128$, $368/128$, $312/128$, and $268/128$. (c) Average magnon distribution change $\delta\langle n\rangle_{\text{FRI}+1\to\text{FRI},l} = \langle n\rangle_{N=L,l} - \langle n\rangle_{N=L-1,l}$ along the chain as a function of unit cell l shows the presence of the edge states for the four chains studied. (d) The average magnon probability density $\langle n\rangle$ along a chain with $L = 128$ at (circles) a and (diamonds) b sites for (white symbols) $N = L - 1$ and (red symbols) $N = L$ bosons from the t-X-V approximation of the $(1/2, 1)$ chain. (e) Sketch of the ground states for $N = L - 1$ and $N = L$ bosons. Average magnon densities are shown as gray circles, fluctuations between a and b sites are indicated by a blue stripe, and we use a red filled curve to represent the localized orbital in the boundary unit cell.

with the magnon average higher on a sites than on b sites. Quantum fluctuations between a and b sites in nearby unit cells are expected, given the excellent accordance between the results from the t-X-V approximation and the spin model in the high-density limit, $m \to m_{\text{FRI}}$. Adding one magnon to the $(L-1)$-magnon state, we obtain the magnetization at $m = S - s$ in the finite-size system, which is also an insulating state. The added magnon occupies the empty localized orbital state in the unit cell of the boundary a site. The penetration of this edge state in the gapped bulk is very tiny and decreases with increasing S, see Fig. 5(c), as can be estimated through the average magnon distribution.

IV. THE RELEVANCE OF THE BOUNDARY POTENTIALS AND INTERACTIONS IN THE BOUNDARY MAGNON DENSITY OF THE BOSONIC MODEL

With the help of Fig. 6, we discuss the relevance of the difference between the local potential in the boundaries and the bulk sites on the boundary magnon densities, as well as the importance of interactions in it. We use the parameters of the spin-$(1/2, 1)$ chain but focus on the bosonic Hamiltonian, for three models in finite-size chains: (1) the interacting model considering the mapping to the spin system $(X \neq 0, V \neq 0)$, the t-X-V model; (2) the corresponding noninteracting model,

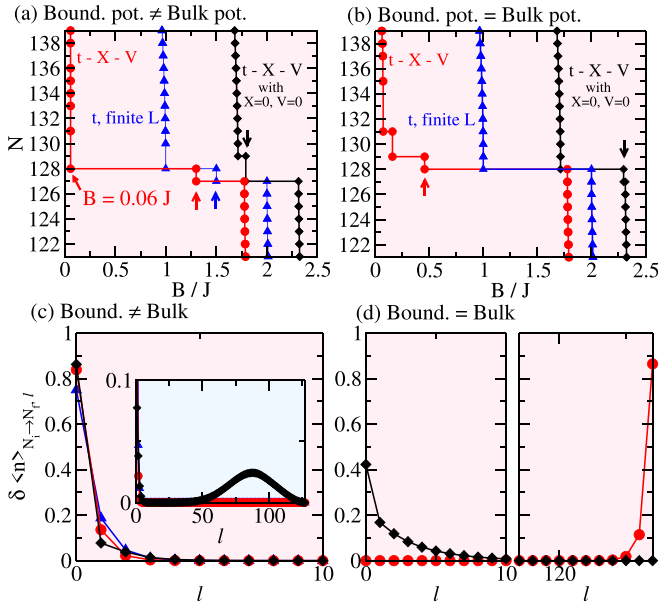

FIG. 6. DMRG results for finite-size modified Rice-Mele models with $L = 128$. In (a) and (c), the boundary potentials have the values in Eq. (9), while in (b) and (d), the boundary potentials have the same values of the bulk local potentials on a and b sites, ε_a and ε_b in Eq. (8). Taking the parameters from the spin-(1/2, 1) chain, we show data for the full interacting model, t-X-V, the t-X-V model with $X = 0 = V$, and the hard-core approximation t. In (a) and (b), we present the number of magnons N as a function of magnetic field (in units of J) $B = -\mu$, where μ is the chemical potential in the bosonic system. In (c) and (d), we show the change in magnon density per unit cell $\delta\langle n\rangle_{N_i\to N_f,l} = \langle n\rangle_{N_f,l} - \langle n\rangle_{N_i,l}$ between states $N = N_i$ and $N = N_f$ as a function of unit cell l, where the arrows in (a) and (b) identify N_i and N_f for each model.

i.e., the t-X-V model with $X = 0$ and $V = 0$, which has a hard-core constraint on a sites and the b sites can host up to two bosons; (3), the t approximation, which has a hard-core constraint on a and b sites. One of the sets, Figs. 6(a) and 6(c), shows data for the boundary potentials distinct from the bulk potentials, with the values in Eqs. (9) and (8), respectively. The other set, Figs. 6(b) and 6(d), takes the value of the boundary potentials equal to the bulk ones, Eq. (8). The arrows in Figs. 6(a) and 6(b) indicate the edge states whose boson density change

$$\delta\langle n\rangle_{N_i\to N_f,l} = \langle n\rangle_{N_f,l} - \langle n\rangle_{N_i,l} \tag{34}$$

is shown in Figs. 6(c) and 6(d), respectively, where N_f (N_i) is the highest (lowest) value of N between the two magnon density steps separated by the occupancy of the edge state. For the bulk different from the boundaries, Fig. 6(a), we see that the edge state is very robust, appearing even in the t approximation. This does not occur for the t approximation if the boundary is equal to the bulk, Fig. 6(b), which is an expected result for the Rice-Mele model [83]. However, we notice in Fig. 6(a) that in comparison with the spin model, the plateau width is very underestimated in the t approximation, since we are not discarding the single-particle states in the upper band shown in Fig. 2. We observe that this upper band was discarded for the $L \to \infty$ results shown in Figs. 3 and 4, due to the introduction of the effective chemical potential connected with the Takhashi's constraint [64]. Considering also the spin model, the error in the plateau width for the t-X-V interacting case is very tiny, with a lower critical field $\approx 0.06J$. Also in Fig. 6(a), bulk and boundaries distinct, we note that the edge state in the noninteracting t-X-V model appears only for two bosons over the $N = 127$ state, Fig. 6(a), with one of the bosons occupying an extended state and the other an edge state, as shown in Fig. 6(c). This shows that the distinction between boundaries and bulk is not sufficient to a good representation of the edge state in the spin mode; the *interactions* are essential for it. In the case of the t approximation, the particle statistics provide a change in the single particle quantum states that mimic the effect of the X and V interactions in the t-X-V model. In Fig. 6(b), where the boundary is equal to the bulk, we show that edge states appear in the t-X-V model in the interacting and noninteracting cases. As mentioned above, the edge state of the noninteracting case does not appear in the t approximation. Further, the boundary density, Fig. 6(d), in the interacting t-X-V case appears in the right extreme and has a value approximately equal to that in Fig. 6(c). From these results, we can assert that the interactions X and V, and the particle statistics, are essential to understand the boundary magnon density.

V. SUMMARY AND DISCUSSION

We have investigated the Holstein-Primakoff bosonic Hamiltonian, up to order $\sqrt{s/S}$, of the alternating spin-($s = 1/2$, S) chains in a magnetic field, considering the fully polarized as the vacuum. Three bosonic Hamiltonians were considered: The first has only a hopping term (t approximation) and distinct local potentials (ε) on the spin-1/2 (a site) and the spin-S (b site) sites; this approximation is a Rice-Mele Hamiltonian with boundaries different from the bulk and uniform hopping term. The second one has the terms of the t approximation plus a magnon-magnon repulsion V (t-V approximation), and the last approximation shows the t and V terms and a density-dependent correlated hopping term X (t-X-V approximation). In the t-X-V approximation, b sites can accommodate up to two magnons, while in the others a hard-core constraint is imposed on a and b sites. The local potentials, at any density, and V for higher densities favor magnon localization on the a sites. On the other hand, quantum fluctuations, magnon tunneling between a and b sites, are favored by t, at any density, and X for higher densities. We use the density matrix renormalization group to investigate the spin model and the bosonic Hamiltonians t-V and t-X-V in finite-size open systems, while for the t approximation we have considered its analytical solution. We compare the magnetization and magnon densities per unit cell as a function of a magnetic field, average bulk density, and local densities along the chains from the spin model and the bosonic approximations. From the ferrimagnetic plateau (one magnon per unit cell) to saturation (empty chain), the t-X-V approximation is in excellent agreement with the spin model, while the t and t-V results depart from that of the spin model as the magnon density increases. This, thus, shows the relevance of both interaction terms, magnon-magnon repulsion and the correlated hopping term X, and its associated

particle fluctuations, to describe the many-body system near the ferrimagnetic plateau. The edge state associated with the insulating ferrimagnetic plateau is well reproduced by the bosonic model. In particular, we have shown that the magnon boundary densities are strongly dependent on the interactions and the particle statistics.

The use of the fully polarized state as the vacuum enables a better understanding of the underlying quantum processes in the spin Hamiltonian, compared to a ferrimagnetic vacuum, which is not an exact eigenstate of the spin Hamiltonian. Our results also suggest that, beyond hopping and magnon-magnon interaction, the density-dependent hopping term increases the range of magnetizations for which effective bosonic models can make a good description of the physical data from general spin systems having ions with spins higher than $1/2$.

ACKNOWLEDGMENTS

We acknowledge support from Coordenação de Aperfeiçoamento de Pessoal de Nível Superior (CAPES), Conselho Nacional de Desenvolvimento Científico e Tecnológico (CNPq), and Fundação de Amparo à Ciência e Tecnologia do Estado de Pernambuco (FACEPE), Brazilian agencies, including the PRONEX Program which is funded by CNPq and FACEPE, Grant No. APQ-0602-1.05/14.

[1] T. Giamarchi, C. Rüegg, and O. Tchernyshyov, Bose-Einstein condensation in magnetic insulators, Nat. Phys. **4**, 198 (2008).

[2] M. Oshikawa, M. Yamanaka, and I. Affleck, Magnetization Plateaus in Spin Chains: "Haldane Gap" for Half-Integer Spins, Phys. Rev. Lett. **78**, 1984 (1997).

[3] H. Hu, C. Cheng, Z. Xu, H.-G. Luo, and S. Chen, Topological nature of magnetization plateaus in periodically modulated quantum spin chains, Phys. Rev. B **90**, 035150 (2014); H.-P. Hu, C. Cheng, H.-G. Luo, and S. Chen, Topological incommensurate magnetization plateaus in quasi-periodic quantum spin chains, Sci. Rep. **5**, 8433 (2015).

[4] T. Giamarchi, *Quantum Physics in One Dimension* (Oxford University Press, Oxford, 2004); R. Chitra and T. Giamarchi, Critical properties of gapped spin-chains and ladders in a magnetic field, Phys. Rev. B **55**, 5816 (1997).

[5] S. Sachdev, *Quantum Phase Transitions* (Cambridge University Press, Cambridge, 2001).

[6] M. Vojta, Quantum phase transitions, Rep. Prog. Phys. **66**, 2069 (2003).

[7] I. Affleck, Bose condensation in quasi-one-dimensional antiferromagnets in strong fields, Phys. Rev. B **43**, 3215 (1991).

[8] E. S. Sørensen and I. Affleck, Large-Scale Numerical Evidence for Bose Condensation in the $S = 1$ Antiferromagnetic Chain in a Strong Field, Phys. Rev. Lett. **71**, 1633 (1993).

[9] A. M. Tsvelik, Field-theory treatment of the Heisenberg spin-1 chain, Phys. Rev. B **42**, 10499 (1990).

[10] K. Okunishi, Y. Hieida, and Y. Akutsu, δ-function Bose-gas picture of $S = 1$ antiferromagnetic quantum spin chains near critical fields, Phys. Rev. B **59**, 6806 (1999).

[11] J. Lou, S. Qin, T.-K. Ng, Z. Su, and I. Affleck, Finite-size spectrum, magnon interactions, and magnetization of $S = 1$ Heisenberg spin chains, Phys. Rev. B **62**, 3786 (2000).

[12] I. Affleck, W. Hofstetter, D. R. Nelson, and U. Schollwöck, Non-Hermitian Luttinger liquids and flux line pinning in planar superconductors, J. Stat. Mech.: Theory Exp. (2004) P10003.

[13] I. Affleck, Luttinger liquid parameter for the spin-1 Heisenberg chain in a magnetic field, Phys. Rev. B **72**, 132414 (2005).

[14] L. Vanderstraeten, F. Verstraete, and J. Haegeman, Scattering particles in quantum spin chains, Phys. Rev. B **92**, 125136 (2015).

[15] A. Dobry and A. Aligia, Quantum phase diagram of the half filled Hubbard model with bond-charge interaction, Nucl. Phys. B **843**, 767 (2011).

[16] S. Kivelson, W.-P. Su, J. R. Schrieffer, and A. J. Heeger, Missing Bond-Charge Repulsion in the Extended Hubbard Model: Effects in Polyacetylene, Phys. Rev. Lett. **58**, 1899 (1987).

[17] J. Hirsch, Bond-charge repulsion and hole superconductivity, Physica C: Superconduct. Appl. **158**, 326 (1989).

[18] J. E. Hirsch and F. Marsiglio, Superconducting state in an oxygen hole metal, Phys. Rev. B **39**, 11515 (1989).

[19] G. I. Japaridze and A. P. Kampf, Weak-coupling phase diagram of the extended Hubbard model with correlated-hopping interaction, Phys. Rev. B **59**, 12822 (1999).

[20] J. Vidal and B. Douçot, Strongly correlated hopping and many-body bound states, Phys. Rev. B **65**, 045102 (2001).

[21] A. Anfossi, P. Giorda, and A. Montorsi, Entanglement in extended Hubbard models and quantum phase transitions, Phys. Rev. B **75**, 165106 (2007).

[22] L. Arrachea and A. A. Aligia, Exact Solution of a Hubbard Chain with Bond-Charge Interaction, Phys. Rev. Lett. **73**, 2240 (1994).

[23] A. Schadschneider, Superconductivity in an exactly solvable Hubbard model with bond-charge interaction, Phys. Rev. B **51**, 10386 (1995).

[24] F. Dolcini and A. Montorsi, Finite-temperature properties of the Hubbard chain with bond-charge interaction, Phys. Rev. B **66**, 075112 (2002).

[25] C. Vitoriano and M. D. Coutinho-Filho, Fractional Statistics and Quantum Scaling Properties of the Hubbard Chain with Bond-Charge Interaction, Phys. Rev. Lett. **102**, 146404 (2009).

[26] M. Maik, P. Hauke, O. Dutta, M. Lewenstein, and J. Zakrzewski, Density-dependent tunneling in the extended Bose-Hubbard model, New J. Phys. **15**, 113041 (2013).

[27] S. Baier, M. J. Mark, D. Petter, K. Aikawa, L. Chomaz, Z. Cai, M. Baranov, P. Zoller, and F. Ferlaino, Extended Bose-Hubbard models with ultracold magnetic atoms, Science **352**, 201 (2016).

[28] S. Fazzini, A. Montorsi, M. Roncaglia, and L. Barbiero, Hidden magnetism in periodically modulated one dimensional dipolar fermions, New J. Phys. **19**, 123008 (2017).

[29] R. Bendjama, B. Kumar, and F. Mila, Absence of Single-Particle Bose-Einstein Condensation at Low Densities for Bosons with Correlated Hopping, Phys. Rev. Lett. **95**, 110406 (2005).

[30] K. P. Schmidt, J. Dorier, A. Läuchli, and F. Mila, Single-particle versus pair condensation of hard-core bosons with correlated hopping, Phys. Rev. B **74**, 174508 (2006).

[31] K. P. Schmidt, J. Dorier, A. M. Läuchli, and F. Mila, Supersolid Phase Induced by Correlated Hopping in Spin-1/2 Frustrated Quantum Magnets, Phys. Rev. Lett. **100**, 090401 (2008).

[32] M. Eckholt and J. J. García-Ripoll, Correlated hopping of bosonic atoms induced by optical lattices, New J. Phys. **11**, 093028 (2009).

[33] H. C. Jiang, L. Fu, and C. Xu, Pair superfluid and supersolid of correlated hard-core bosons on a triangular lattice, Phys. Rev. B **86**, 045129 (2012).

[34] O. Jürgensen, F. Meinert, M. J. Mark, H.-C. Nägerl, and D.-S. Lühmann, Observation of Density-Induced Tunneling, Phys. Rev. Lett. **113**, 193003 (2014).

[35] K. Biedroń, M. Łaącki, and J. Zakrzewski, Extended Bose-Hubbard model with dipolar and contact interactions, Phys. Rev. B **97**, 245102 (2018).

[36] D. Johnstone, N. Westerberg, C. W. Duncan, and P. Öhberg, Staggered ground states in an optical lattice, Phys. Rev. A **100**, 043614 (2019).

[37] J. Stasińska, R. W. Chhajlany, O. Dutta, and M. Lewenstein, Effects of extended correlated hopping in a bose-bose mixture, arXiv:1912.13359.

[38] E. Lieb and D. Mattis, Ordering energy levels of interacting spin systems, J. Math. Phys. **3**, 749 (1962).

[39] G.-S. Tian, Coexistence of the ferromagnetic and antiferromagnetic long-range orders in the generalized antiferromagnetic heisenberg model on a bipartite lattice, J. Phys. A: Math. Gen. **27**, 2305 (1994).

[40] E. P. Raposo and M. D. Coutinho-Filho, Quantum Critical Properties of Ferrimagnetic Hubbard Chains, Phys. Rev. Lett. **78**, 4853 (1997); Field theory of ferrimagnetic hubbard chains, Phys. Rev. B **59**, 14384 (1999).

[41] F. C. Alcaraz and A. L. Malvezzi, Critical behavior of mixed heisenberg chains, J. Phys. A: Math. Gen. **30**, 767 (1997).

[42] B. Gu, G. Su, and S. Gao, Thermodynamics of spin-1 2 antiferromagnet-antiferromagnet-ferromagnet and ferromagnet-ferromagnet-antiferromagnet trimerized quantum Heisenberg chains, Phys. Rev. B **73**, 134427 (2006); S.-S. Gong, S. Gao, and G. Su, Thermodynamics of spin-1/2 tetrameric Heisenberg antiferromagnetic chain, *ibid.* **80**, 014413 (2009); S.-S. Gong, W. Li, Y. Zhao, and G. Su, Magnetism and thermodynamics of spin-(1/2, 1) decorated Heisenberg chain with spin-1 pendants, *ibid.* **81**, 214431 (2010).

[43] T. Sakai and S. Yamamoto, Critical behavior of anisotropic Heisenberg mixed-spin chains in a field, Phys. Rev. B **60**, 4053 (1999).

[44] L. M. Veríssimo, M. S. S. Pereira, J. Strečka, and M. L. Lyra, Kosterlitz-Thouless and Gaussian criticalities in a mixed spin-(1/2, 5/2, 1/2) branched chain with exchange anisotropy, Phys. Rev. B **99**, 134408 (2019).

[45] R. R. Montenegro-Filho, F. S. Matias, and M. D. Coutinho-Filho, Topology of many-body edge and extended quantum states in an open spin chain: 1/3 plateau, Kosterlitz-Thouless transition, and Luttinger liquid, Phys. Rev. B **102**, 035137 (2020).

[46] A. M. S. Macêdo, M. C. dos Santos, M. D. Coutinho-Filho, and C. A. Macêdo, Magnetism and Phase Separation in Polymeric Hubbard Chains, Phys. Rev. Lett. **74**, 1851 (1995).

[47] R. R. Montenegro-Filho and M. D. Coutinho-Filho, Doped ab_2 hubbard chain: Spiral, nagaoka and resonating-valence-bond states, phase separation, and luttinger-liquid behavior, Phys. Rev. B **74**, 125117 (2006).

[48] G. Sierra, M. A. Martín-Delgado, S. R. White, D. J. Scalapino, and J. Dukelsky, Diagonal ladders: A class of models for strongly coupled electron systems, Phys. Rev. B **59**, 7973 (1999).

[49] R. R. Montenegro-Filho and M. D. Coutinho-Filho, Magnetic and nonmagnetic phases in doped AB_2 t-j hubbard chains, Phys. Rev. B **90**, 115123 (2014).

[50] K. Kobayashi, M. Okumura, S. Yamada, M. Machida, and H. Aoki, Superconductivity in repulsively interacting fermions on a diamond chain: Flat-band-induced pairing, Phys. Rev. B **94**, 214501 (2016).

[51] K. Hida, Magnetic properties of the spin-1/2 ferromagnetic-ferromagnetic-antiferromagnetic trimerized heisenberg chain, J. Phys. Soc. Jpn. **63**, 2359 (1994).

[52] K. Takano, K. Kubo, and H. Sakamoto, Ground states with cluster structures in a frustrated Heisenberg chain, J. Phys.: Condens. Matter **8**, 6405 (1996).

[53] R. R. Montenegro-Filho and M. D. Coutinho-Filho, Frustration-induced quantum phase transitions in a quasi-one-dimensional ferrimagnet: Hard-core boson map and the tonks-girardeau limit, Phys. Rev. B **78**, 014418 (2008).

[54] N. B. Ivanov, Spin models of quasi-1d quantum ferrimagnets with competing interactions, Condens. Matter Phys. **12**, 435 (2009).

[55] T. Shimokawa and H. Nakano, Frustration-Induced Ferrimagnetism in $S = 1/2$ Heisenberg Spin Chain, J. Phys. Soc. Jpn. **80**, 043703 (2011).

[56] S. C. Furuya and T. Giamarchi, Spontaneously magnetized Tomonaga-Luttinger liquid in frustrated quantum antiferromagnets, Phys. Rev. B **89**, 205131 (2014).

[57] F. Amiri, G. Sun, H. J. Mikeska, and T. Vekua, Ground-state phases of a rung-alternated spin- 12 Heisenberg ladder, Phys. Rev. B **92**, 184421 (2015).

[58] K. Sekiguchi and K. Hida, Partial Ferrimagnetism in $S = 1/2$ Heisenberg Ladders with a Ferromagnetic Leg, an Antiferromagnetic Leg, and Antiferromagnetic Rungs, J. Phys. Soc. Jpn. **86**, 084706 (2017).

[59] S. K. Pati, S. Ramasesha, and D. Sen, A density matrix renormalization group study of low-energy excitations and low-temperature properties of alternating spin systems, J. Phys.: Condens. Matter **9**, 8707 (1997); Low-lying excited states and low-temperature properties of an alternating spin-1–spin-1/2 chain: A density-matrix renormalization-group study, Phys. Rev. B **55**, 8894 (1997).

[60] K. Maisinger, U. Schollwöck, S. Brehmer, H. J. Mikeska, and S. Yamamoto, Thermodynamics of the (1, 1/2) ferrimagnet in finite magnetic fields, Phys. Rev. B **58**, R5908 (1998).

[61] A. S. F. Tenório, R. R. Montenegro-Filho, and M. D. Coutinho-Filho, Quantum phase transitions in alternating spin-1/2–spin-5/2 heisenberg chains, J. Phys.: Condens. Matter **23**, 506003 (2011).

[62] J. Strečka and T. Verkholyak, Magnetic Signatures of Quantum Critical Points of the Ferrimagnetic Mixed Spin-(1/2, S)

Heisenberg Chains at Finite Temperatures, J. Low Temp. Phys. **187**, 712 (2017).

[63] J. Strečka, Breakdown of a Magnetization Plateau in Ferrimagnetic Mixed Spin-(1/2,S) Heisenberg Chains due to a Quantum Phase Transition towards the Luttinger Spin Liquid, Acta Phys. Pol. A **131**, 624 (2017).

[64] W. M. da Silva and R. R. Montenegro-Filho, Magnetic-field-temperature phase diagram of alternating ferrimagnetic chains: Spin-wave theory from a fully polarized vacuum, Phys. Rev. B **96**, 214419 (2017).

[65] M. Hagiwara, K. Minami, Y. Narumi, K. Tatani, and K. Kindo, Magnetic Properties of a Quantum Ferrimagnet: NiCu(pba)(D 2 O) 3 2 D 2 O, J. Phys. Soc. Jpn. **67**, 2209 (1998).

[66] M. Hagiwara, Y. Narumi, K. Minami, K. Tatani, and K. Kindo, Magnetization Process of the $S = 1/2$ and 1 Ferrimagnetic Chain and Dimer, J. Phys. Soc. Jpn. **68**, 2214 (1999).

[67] O. Kahn, Y. Pei, M. Verdaguer, J. P. Renard, and J. Sletten, Magnetic ordering of manganese(II) copper(II) bimetallic chains; design of a molecular based ferromagnet, J. Am. Chem. Soc. **110**, 782 (1988).

[68] A. Gleizes and M. Verdaguer, Ordered magnetic bimetallic chains: A novel class of one-dimensional compounds, J. Am. Chem. Soc. **103**, 7373 (1981).

[69] M. Verdaguer, A. Gleizes, J. P. Renard, and J. Seiden, Susceptibility and magnetization of $CuMn(S_2C_2O_2)_2 \cdot 7.5H_2O$, Phys. Rev. B **29**, 5144 (1984).

[70] P. J. Van Koningsbruggen, O. Kahn, K. Nakatani, Y. Pei, J. P. Renard, M. Drillon, and P. Legoll, Magnetism of A-copper(II) bimetallic chain compounds (A = iron, cobalt, nickel): One- and three-dimensional behaviors, Inorg. Chem. **29**, 3325 (1990).

[71] H. Yamaguchi, T. Okita, Y. Iwasaki, Y. Kono, N. Uemoto, Y. Hosokoshi, T. Kida, T. Kawakami, A. Matsuo, and M. Hagiwara, Experimental realization of Lieb-Mattis plateau in a quantum spin chain, Sci. Rep. **10**, 9193 (2020); H. Yamaguchi, Y. Iwasaki, Y. Kono, T. Okita, A. Matsuo, M. Akaki, M. Hagiwara, and Y. Hosokoshi, Low-energy magnetic excitations in the mixed spin-(1/2, 5/2) chain, Phys. Rev. B **102**, 060408(R) (2020).

[72] Y. Noriki and S. Yamamoto, Modified Spin-Wave Theory on Low-Dimensional Heisenberg Ferrimagnets: A New Robust Formulation, J. Phys. Soc. Jpn. **86**, 034714 (2017).

[73] S. Brehmer, H.-J. Mikeska, and S. Yamamoto, Low-temperature properties of quantum antiferromagnetic chains with alternating spins and, J. Phys.: Condens. Matter **9**, 3921 (1997).

[74] S. Yamamoto and T. Fukui, Thermodynamic properties of heisenberg ferrimagnetic spin chains: Ferromagnetic-antiferromagnetic crossover, Phys. Rev. B **57**, R14008 (1998).

[75] S. Yamamoto, S. Brehmer, and H.-J. Mikeska, Elementary excitations of heisenberg ferrimagnetic spin chains, Phys. Rev. B **57**, 13610 (1998).

[76] S. Yamamoto, T. Fukui, K. Maisinger, and U. Schollwöck, Combination of ferromagnetic and antiferromagnetic features in heisenberg ferrimagnets, J. Phys.: Condens. Matter **10**, 11033 (1998).

[77] N. B. Ivanov, Magnon dispersions in quantum Heisenberg ferrimagnetic chains at zero temperature, Phys. Rev. B **62**, 3271 (2000).

[78] S. Yamamoto, Bosonic representation of one-dimensional heisenberg ferrimagnets, Phys. Rev. B **69**, 064426 (2004).

[79] S. R. White, Density-matrix algorithms for quantum renormalization groups, Phys. Rev. B **48**, 10345 (1993).

[80] S. R. White, Density Matrix Formulation for Quantum Renormalization Groups, Phys. Rev. Lett. **69**, 2863 (1992).

[81] M. J. Rice and E. J. Mele, Elementary Excitations of a Linearly Conjugated Diatomic Polymer, Phys. Rev. Lett. **49**, 1455 (1982).

[82] N. R. Cooper, J. Dalibard, and I. B. Spielman, Topological bands for ultracold atoms, Rev. Mod. Phys. **91**, 015005 (2019).

[83] Y.-T. Lin, D. M. Kennes, M. Pletyukhov, C. S. Weber, H. Schoeller, and V. Meden, Interacting Rice-Mele model: Bulk and boundaries, Phys. Rev. B **102**, 085122 (2020).

[84] M. Takahashi, Few-Dimensional Heisenberg Ferromagnets at Low Temperature, Phys. Rev. Lett. **58**, 168 (1987).

[85] B. Bauer, L. D. Carr, H. G. Evertz, A. Feiguin, J. Freire, S. Fuchs, L. Gamper, J. Gukelberger, E. Gull, S. Guertler, A. Hehn, R. Igarashi, S. V. Isakov, D. Koop, P. N. Ma, P. Mates, H. Matsuo, O. Parcollet, G. Pawłowski, J. D. Picon, L. Pollet, E. Santos, V. W. Scarola, U. Schollwöck, C. Silva, B. Surer, S. Todo, S. Trebst, M. Troyer, M. L. Wall, P. Werner, and S. Wessel, The ALPS project release 2.0: open source software for strongly correlated systems, J. Stat. Mech.: Theory Exp. (2011) P05001.

[86] T. Sakai and S. Yamamoto, Coexistent quantum and classical aspects of magnetization plateaux in alternating-spin chains, J. Phys.: Condens. Matter **12**, 9787 (2000).